Dynamic simulation of sediment films of Yukawa-stabilized particles

Damien D. Brewer and Satish Kumar

Phys. Rev. E **91**, 022304 — Published 13 February 2015

DOI: 10.1103/PhysRevE.91.022304

Dynamic simulation of sediment films of Yukawa-stabilized particles

Damien D. Brewer, Satish Kumar

Department of Chemical Engineering and Materials Science
University of Minnesota, Minneapolis, MN 55455

Abstract

The fast lubrication dynamics method is applied to simulate the motion and deposition of charge-stabilized 100 nm diameter particles into sediment films from aqueous dispersions. Colloidal interactions are incorporated with a Yukawa potential, and the effects of the screened-Coulomb potential strength and Péclet number (which controls the sedimentation driving force) on particle orientation are quantified with a 6-fold bond order parameter. The effect of sediment growth rate on the order parameter is determined and related back to a competition between the electrostatic interaction strength and sedimentation driving force. Increasing the electrostatic interaction strength and decreasing the Péclet number lead to lower sediment growth rates and consequently greater 6-fold bond order. Our work demonstrates the feasibility of including lubrication interactions in dynamic simulations of sediment films, and suggests that these interactions play a central role in the kinetics of film microstructure development and consequently on the degree of order within the film.

.

I. Introduction

Technologically important colloidal particle films include coalesced latex overcoats, paints, and adhesives; semiconducting transparent reflective or anti-reflective layers; toners and cosmetics; and sintered conductive inks. Commercial initiatives in assembled films for photonics and biotechnology are presently underway, though assembly of precisely tuned optical and electronic films has yet to make large-scale technological inroads. One of several hindering factors in this regard is the process rate: the modular or roll-to-roll processed film is preferably realized at linear velocities on the order of 1 m/s, far more quickly than capillarity at a receding contact line has been shown to arrange long-range-ordered particle films.[1] Nevertheless, attention in this area is deserved because of its relation to condensed atomic systems and for the fact that the desired structure is thermodynamically favored.[2]

In aqueous systems the particle size contributes to the nature of assembly, whether kinetically driven or one in which annealing to energetic minima is possible. In a sedimentation process, the competition between convective effects and Brownian motion is characterized by the Péclet number (Pe),

$$\mathrm{Pe}=\frac{\mathrm{Ua}}{\mathrm{D}} \qquad (1)$$

where U is the characteristic velocity scale of the sedimentation process, a is the characteristic particle radius, and D is the particle diffusion coefficient. Colloidal film assembly at low Pe has been well studied and is known to generate ordered structures with 6-fold positional symmetry which are useful in templating[3] and as models of atomic crystals.

Low-Pe assembly may also be responsible for the facile assembly of semiconductor nanoparticles into ordered monoliths upon drying of a suspension.[4,5] Additionally, a sequence of studies on the coffee-ring effect beginning with Deegan et al.[6] has identified such relatively slow, low-Pe processes as necessary for colloidal epitaxy.[7] In contrast, the moderate-to-high Péclet number situation – termed "rush-hour" in one report by Marin et al.[7] – was illustrated (using 0.5 to 2.0 μm diameter latex particles) to be deleterious to crystal propagation. Colloidal epitaxy via sedimentation was also quantified by Ramsteiner et al. using confocal microscopy both for un-

templated and templated surfaces[8]. Nevertheless, it is of interest to better understand the moderate-to-high Péclet number regime due to the need for higher fabrication speeds and in some cases small particle diameters (which may be required due to the desired optical, mechanical, and electrical properties of the colloidal film).

In this paper, we examine via dynamic simulations the relationship between film formation rate and local 6-fold bond orientational order of particles sedimenting from electrostatically stabilized aqueous colloidal dispersions. In particular, we determine how a 6-fold bond orientational order parameter and complementary radial distribution functions depend on the screened-Coulomb interaction strength and Péclet number. We also examine the temporal evolution of the sediment-averaged order parameter and spatial variation of the radial distribution functions. A notable feature of this work is the inclusion of lubrication interactions between the colloidal particles, which have not been included in prior dynamic simulations of sediment films to the best of the authors' knowledge. As we will see, our results suggest that these interactions play a central role in the kinetics of film microstructure development and consequently on the degree of order within the film.

II. Simulation model and method

The model consists of an idealized NVT system representing an aqueous dispersion of 490 charge-stabilized 100 nm diameter particles that sediment into a film. The effective sedimentation velocity, or Péclet number, can be viewed as a proxy for forced evaporation-driven particle convection. It is important to understand that the sedimentation velocity is imposed as a free-field bulk motion (velocity) due to external forcing rather than as a sedimentation force. The difference can be appreciated by considering the integrated particle velocities, given by $U = U^{\infty} + (R)^{-1} \cdot (F^B + F^P)$, where U^{∞} is the imposed bulk motion, R is the hydrodynamic resistance matrix, and F^B and F^P are the Brownian force and interparticle-potential force.

Pairwise electrostatic interactions are treated with pairwise Yukawa potentials, yielding a dimensionless force of the form $F_{PP} = {\psi_P}^2 \frac{1+\kappa r}{(r/a)^2} exp\big(-\kappa(r-2a)\big)$, where κ is the inverse Debye length, r is the center-to-center particle separation, and a is the particle radius. Here,

F_{PP} has been made dimensionless with respect to k_BT/a, where k_B is Boltzmann's constant and T is the temperature, while ψ_P represents the (effective) particle potential. The particles deposit irreversibly onto a templated {100} surface composed of discrete particles with in-plane dimensions of $18a$ by $20a$, where upon deposition each particle is fully immobilized. Prior to sedimentation, the particles are initialized in the simulation box by random placement and may assume positions anywhere except those that overlap with the template particles. Upon approaching the surface of discrete particles, suspended particles interact with the surface via pairwise particle-particle potentials of the same form as F_{PP} given above. The relative tendencies toward epitaxial growth are then quantified with an order parameter Q_6, which is a metric for the extent to which a particle packing approaches a long-range symmetry type such as hexagonally close-packed hcp or fcc, with an upper limit of 0.485 for bcc packing and 0.575 for fcc packing.[9]

These simulations employ the fast lubrication dynamics method, in which the exact pairwise sphere-sphere resistance terms to relative particle motion are used while far-field many-body mobility is addressed via an effective isotropic resistance.[10] This model is based on the assertion that the elements of the resistance matrix are dominated by short-range pairwise lubrication forces rather than long-range hydrodynamic forces when the suspension is non-dilute, as well as the assertion that the most important contributions from the far-field mobility matrix are the diagonal elements, which fall off as the inverse particle separation distance rather than the more rapid decay of other mobility components.[11] The model accounts for translational and rotational motion, and has been validated in simple shear flows.[10,12] Figure 1 illustrates a representative sample of particle sedimentation in which a film has deposited on top of the templated {100} surface.

III. Role of hydrodynamic interactions

Before proceeding, we briefly discuss the role played by hydrodynamic interactions in the formation of sediment films. The role played by hydrodynamic interactions in microstructure formation in particle sediments has been studied by Dickinson and co-workers.[13,14] Ansell and Dickinson[13] incorporated long-range hydrodynamic interactions into simulations of particle sedimentation at Pe ~ 2 to 19. Comparing their results with and without such interactions, Ansell

and Dickinson concluded that long-range hydrodynamic interactions enhance sediment packing density at moderate to high Péclet numbers (Pe > 10). The authors rationalize their findings on the basis of a kinetic argument involving competing time scales. When the time for relative motion of a sedimenting particle toward an immobilized particle is shorter than the time to traverse the primary interparticle potential, it accesses a range of potential energy minima and is more likely to anneal at a lower potential energy well. Hydrodynamic interactions were found to be less important at low Pe, at least with regard to packing density. This result may have been due in part to weak primary potential energy barriers that allowed highly dendritic structures to form. Perhaps for this reason, many studies of sedimentation have focused on low-Pe gel formation in the absence of hydrodynamic interactions.[15] However, the more recent results reviewed by Dickinson[14] suggest that that hydrodynamic interactions should play a role in any such kinetically determined process.

While it is widely acknowledged that both long-range and short-range (i.e., lubrication-type) hydrodynamic interactions dictate microstructure formation in dense sheared colloidal dispersions and even in porous media flows,[16] less is known about their roles in particle sediments. Lubrication interactions are expected to become important as particles closely approach each other, which is the case in sediment films. Despite the importance of such short-range hydrodynamic interactions, to the best of our knowledge prior dynamic simulations of sediment films have not accounted for them. Prior Stokesian dynamics simulations of sedimentation have been in unbound domains[17] or considered irreversible deposition of 45 non-Brownian particles without characterizing film ordering.[18]

IV. Orientational order

Prior to presenting the results, we discuss how orientational order is quantified in this work. Local and long-range orientational order (i.e., positional ordering of particles with 6-fold symmetry) is influenced in a qualitatively different manner than in the aforementioned examples of weakly aggregating systems where moderate Pe and interparticle aggregation strength yield the greatest degree of packing density and orientational order. This follows from our imposed requirement that a suspended particle fall into a local "lattice site" defined by mutual adjacency with three previously settled particles in order to become immobilized on the sediment. When a

mobile particle satisfies this mutual adjacency condition ($r_{ij} < 2.008a$), a Metropolis Monte Carlo simulation is run to anneal it in place ($r_{ij} < 2.005a$). In essence the "sticking probability" of one particle to another is lower here than in colloidal systems designed to form gels, and thus this scheme allows us to emphasize simulation of sediment films rather than less spatially confined aggregates. Sedimentation in this manner may occur onto a site defined by three particles that are mutually adjacent themselves or by any other combination of openly spaced particles which create a local trap or site into which a particle may aggregate[12]. Though this process does tend to preclude very low-volume-fraction sediments (we observed values between 0.52 and 0.66), both low- and high- order-parameter structures are obtained.

The order parameter is defined as[9]

$$Q_6 = \left(\frac{4\pi}{13}\sum_{m=-6}^{6}|Q_{6m}|^2\right)^{\frac{1}{2}} \tag{2a}$$

$$Q_{6\mathrm{m}} = \frac{\sum_{i=1}^{N} q6m(i)CN(i)}{\sum_{i=1}^{N} CN(i)} \tag{2b}$$

$$q_{6\mathrm{m}}(i) = \frac{1}{CN(i)}\sum_{j=1}^{CN(i)} Y_{6m}\left(\theta_{ij}, \varphi_{ij}\right). \tag{2c}$$

In the calculation of order parameter Q_6, the number of local pairwise contacts – or bonds – and their orientations are recorded for each particle in the sediment. The local coordination number, CN(i), is defined as the number of bonds ($r_{ij} < 2.005a$) involving particle i where r_{ij} is the center-to-center distance from particle i to an adjacent particle j. Averaged over the particle population, the mean coordination number is 6 as compared with the theoretical maximum of 12. This average CN arises directly from the imposed three-fold mutual adjacency condition for a deposition event since kinetic arrest precludes additional bond formation. It should be noted that the density of bonds, or average CN, does not directly determine Q_6. Since the order-parameter determination is normalized to the number of bonds, only their relative orientations are registered in the computation according to Eq. 2c. Because the spherical harmonic functions Y_{6m} are generally complex-valued, both q_{6m} and Q_{6m} are complex as well. In this representation, all

bonds constructively interfere when arranged in six-fold symmetry ($\pi/3$ pitch) and to a lesser extent in other symmetries. These local coordination-number normalized bond interactions from Eq. 2c are aggregated over the entire N-particle assembly and normalized with respect to the entire sphere packing in Eq. 2b. The magnitudes of these interactions in Eq. 2a yield an orientation-invariant order parameter.

V. Results

Figure 2a shows the behavior of the order parameter, Q_6, as a function of Pe and particle potential, ψ_p, at $\kappa a = 5$. The maximum value of Q_6, under fcc packing, is 0.575. Marked beside each data point is the order parameter value at the end of the simulation averaged over four simulations. Dashed lines are drawn to indicate regions of approximately equivalent order parameter.

We note that the simulation time was not constant across all samples, nor was the number of particles deposited at the end of a simulation. This is due to the fact that deposition rates varied widely over the simulation timescale, which was always at least 10 times the "convection time" H/Pe, where H is the simulation box height. In order to account for these differences, we extracted long-time-limit estimates of Q_6 by fitting the time-series data with an asymptotic power-law of the form $Q_6(t) - Q_{6,\infty} = kt^{-1/6}$, which we determined empirically. The deviation between $Q_6(t)$ at the end of the simulation and $Q_{6,\infty}$ was typically around 0.03 to 0.05; nevertheless, these values are dependent on the choice of power-law and so represent only an estimate for the deviation in Q_6 at long times. We note also that the maximum drop in Q_6 upon particle placement is approximately 0.001, which enables us to place an upper bound on the long-time deviation of Q_6 for cases in which all particles have not deposited by the end of simulation: for these data the maximum deviation would be 0.1. So, the overall trends shown in Figure 2a are not qualitatively affected by taking Q_6 at finite simulation times as opposed to a long-time estimate, and vice versa.

The mechanism of colloidal sediment growth with low Q_6 is analogous to the formation of amorphous glassy solids for which $Q_6 = 0$. In principle we expect the least-ordered samples (e.g. $Q_6 < 0.2$) to stem from shallow energetic traps formed by neighboring sets of particles;[19] this

process of energetic trapping is represented in the simulations by immobilization of the particle onto the sediment when it becomes coordinated at once by three sediment particles. In the actual experimental systems, as Pe approaches 0, thermal fluctuations break these shallow traps and enable the annealing via entropic interactions to a thermodynamically favored state.[8] Here, however, the Péclet number is greater than unity so that all particle sediments are kinetically arrested and thus metastable.[7] Yet electrostatic repulsion reduces the probability of local arrest by virtue of raising the pairwise potential energy barrier.[10,12] These considerations of local energetic effects explain the more global variation between the limits of a completely amorphous glass ($Q_6 = 0$) and an orientationally ordered film ($Q_6 \sim 0.5$) reflected in Fig. 2a. (Note that values of Q_6 that we obtain from the simulations do not actually reach these limiting values.) We must emphasize that the Q_6 values presented in Fig. 2a refer to sediment pack averages, and therefore include the template particles. As a consequence, the values presented are higher than what would have been obtained had the template particles been excluded. The issue of local order is addressed with radial distribution functions in Figure 3 below.

The sediment-averaged orientational order Q_6 can be rationalized further by considering the radial distribution function g(r/a). Fig. 2b shows g(r/a) for three instances, labeled A, B, and C in Fig. 2a and corresponding to $Q_6 = 0.171$, 0.300, and 0.368 respectively. These plots represent average values over the entire sediment pack. In all three plots, there is a small "shoulder" that appears to the right of the primary peak; the shoulder appears from $r \approx 2.1a$ to $2.6a$. The height of this shoulder (relative to the primary-peak maximum) increases sequentially from A to C. Shoulders beside the third main peak also become more prominent from samples A to C. These shoulders are a feature of the close-packed crystal, and they correspond to pairwise bonds that are longer than those accounted for in the local coordination number or in the order parameter. We note that the volume fraction increases from approximately 0.54 in sample A to nearly 0.64 and 0.62 in samples B and C, respectively.

In Fig. 3 we plot the in-plane g(r/a) curves resolved layerwise, beginning with the bottom layer of template particles and ascending to the top of the sediment pack. Figures 3a and 3b are taken from the simulations denoted A and C in Fig. 2a, respectively. After the first two layers (template and first sediment layer) the coherence of individual layers fails, leaving radial

distributions with particle contact features represented much more strongly than secondary peaks. The top g(r/a) curves of Fig. 3b show a large secondary peak due to a layer of particles that remains fluidized. Figure 3 therefore suggests a loss of fidelity during film propagation from the base {100} surface. If the shoulders observed in the g(r/a) plots are signatures for the loss of local positional order with 6-fold symmetry, then they also highlight the necessity for additional local annealing to achieve highly ordered films ($Q_6 \sim 0.5$).

The difference between sediments in Figs. 2 and 3 corresponding to $Q_6 = 0.171$ and 0.368 (points A and C of Fig. 2) appears to be the rate of order-parameter decay. Figure 4 shows a plot of Q_6 as a function of the sediment pack height, h/a, for these two cases. The data were sampled at regular intervals during the simulation. The first few sedimenting particles break the 4-fold symmetry of the underlying {100} template, resulting in an initial drop in Q_6. The first layer then establishes positional order with 6-fold symmetry, and the order parameter increases through the first layer. Subsequent layers fail to propagate the sediment under 6-fold symmetry in the absence of additional annealing, and Q_6 slowly decreases with sediment packing thickness. In several places the order parameter decreases as an individual layer is being completed, as indicated by vertical "streaks" on Fig. 4. As suggested above it is the rate at which the order-parameter decay occurs that distinguishes the samples. The temporal evolution of Q_6 is shown in Figs. 4c and 4d, corresponding respectively to the simulations of Figs. 4a and 4b. In both cases, there is an initial transient period followed by an approach to steady state. The case with the higher value of Q_6 (Fig. 4d) takes longer to reach steady state. While we observe a fit of the asymptotic power law to order-parameter data (as discussed above), we cannot rule out the possibility that a much larger system ($N \sim 10{,}000$ particles) might demonstrate a propensity toward entirely amorphous behavior.

We expect that the effective rate at which particles sediment is determined by the competing effects of convection (Pe) and screened Coulomb potential strength (ψ_p), with respect to the rate at which particles deposit once they fall into the "energetic traps" created by surrounding sediment particles. The rate of particle deposition is[20]

$$j_n A = \frac{M c_S}{\int_a^\infty \frac{exp(\Phi/k_B T)}{z^2} dz} \quad (3)$$

where j_n is the local particle flux over a cross-section of area A, M is the z-directional particle mobility at the sediment surface, c_S is the number concentration of particles at the surface, z is the direction of deposition, k_B is Boltzmann's constant, and T is the temperature. The potential field Φ pertinent to Eq. (3) is a superposition of external convection and particle potentials, ${\Phi}/{k_B T} = (Pe)\left(\frac{z}{a}\right) + {\psi_P}^2 \left(\frac{a}{z}\right) exp\left(-\kappa(z-a)\right)$. Equation 3 quantifies the rate at which the random Brownian force overcomes the repulsive electrostatic potential field of the sediment with the assistance of a uniform convective driving force.

In the related rate process of flocculation and coagulation of electrostatically stabilized colloidal dispersions, the fractal structure and crystallinity of aggregated particles is defined by the assembly rate of Eq. 3. In a similar fashion, we expect the order parameter Q_6 measured in an NVT system to diminish as the sediment deposition rate j_n increases. Since j_n varies with time, we take as our metric the "early time" sedimentation rate, defined as the average rate during the initial stage of particle sedimentation. Within this regime of the simulation the number of deposited particles increases linearly with time (before entering a regime of diminishing sedimentation rate). This trend is shown in Fig. 5 as a plot of order parameter versus the early-time particle sedimentation flux, j_n, over the area of deposition A. Structures with relatively high Q_6 (greater than 0.3) are clearly favored at low j_n, as suggested by recent work of Marin et al.[7] Rather than examining the role of Péclet number alone, however, these results represent the convection/screened-Coulomb interaction of Fig. 2a. Thus, as expected from the work of Marin et al.,[7] relatively high crystallinity states are achieved by tuning the screening strength up as the Péclet number increases. Conversely, the relatively glassy, amorphous sediments are achieved with low screening strength and a moderate or high convective external driving force for sedimentation.

VI. Conclusions

To the best of the authors' knowledge, this study is the first to account for lubrication interactions in the formation of sediment films, a step which was made feasible by employing the fast

lubrication dynamics method. The kinetics of sedimentation have been shown here to be centrally relevant to positional bond order of 6-fold symmetry, thus making the mobility effects of hydrodynamic interactions relevant as well. While exploration of additional screening lengths κa is outside the scope of this work, it seems likely that a reduction in the screening length would have similar qualitative effects as the reduction in particle potential. Russel et al.[20] have reviewed theories of particle stability and the role of hydrodynamics on Brownian and convection-driven deposition kinetics. Equation 3 indicates that a lower particle mobility leads to a lower sedimentation flux, and Fig. 3 shows that lower fluxes lead to more ordered films. Because lubrication interactions tend to lower particle mobility, our results suggest that inclusion of such interactions leads to more ordered films. Thus we conclude that hydrodynamic interactions not only influence sediment packing density, as Ansell and Dickinson[13] contended, but also play a role in the microstructural development of sediment films. In particular, they would be expected to influence the degree of crystalline order obtained in films of several layers and possibly in much thicker films.

Acknowledgement

D.D.B. gratefully acknowledges support from the NSF Graduate Fellowship Program and a University of Minnesota Doctoral Dissertation Fellowship. We are also grateful to the University of Minnesota for financial support from the Industrial Partnership for Research in Interfacial and Materials Engineering, as well as for computational support and resources provided by the Minnesota Supercomputing Institute.

References

1. S. Maenosono, T. Okubo, and Y. Yamaguchi, J. Nanoparticle Research **5**, 5 (2003).
2. L. Woodcock, Nature **385**, 141 (1997).
3. A. Stein and R. Schroden, Current Opinion in Solid State and Mat. Sci. **5**, 553 (2001).

4. T. P. Bigioni, X.-M. Lin, T. T. Nguyen, E. I. Corwin, T. A. Witten, and H. M. Jaeger, Nature Mat. **5**, 265 (2006).

5. W. Fan, M. A. Snyder, S. Kumar, P.-S. Lee, W. C. Yoo, A. V. McCormick, R. L. Penn, A. Stein, and M. Tsapatsis, Nature Mat. **7**, 984 (2008).

6. R. D. Deegan, Phys. Rev. E **61**, 475 (2000).

7. A. G. Marin, H. Gelderblom, D. Lohse, J. H. Snoeijer, Phys. Rev. Lett. **107**, 085502 (2011).

8. I. B. Ramsteiner, K. E. Jensen, D. A. Weitz, and F Spaepen, Phys. Rev. E **79**, 011403 (2009).

9. P. Wolde, M. J. Ruiz-Montero, and D. Frenkel, J. Chem. Phys. **104**, 9932 (1996).

10. A. Kumar and J. L. Higdon, Phys. Rev. E **82**, 051401 (2010).

11. L. Silbert, J. R. Melrose, R.C. Ball, Phys. Rev. E **56**, 7067 (1997).

12. Brewer, D. Ph.D. Thesis, University of Minnesota, 2011.

13. G. C. Ansell and E. Dickinson, J. Chem. Phys. **85**, 4079 (1986).

14. E. Dickinson, Adv. Colloid Interface Sci. **199**, 114 (2013).

15. J. K. Whitmer and E. Luijten, J. Chem. Phys. 134, 034510 (2011).

16. S. Vitthal and M. M. Sharma, J. Colloid Interface Sci. **153**, 314 (1992).

17. L. Durlofsky, J. F. Brady, and G. Bossis, J. Fluid Mech. 180, 21 (1987).

18. B. Cichocki, R. B. Jones, R. Kutteh, and E. Wajnryb, J. Chem. Phys. 112, 2548 (2000).

19. P. N. Pusey and W. van Megen, Phys. Rev. Lett. **59**, 2083 (1987).

20. W. B. Russel, D. A. Saville, and W. R. Schowalter, Colloidal Dispersions (Cambridge University Press, Cambridge, UK, 1991).

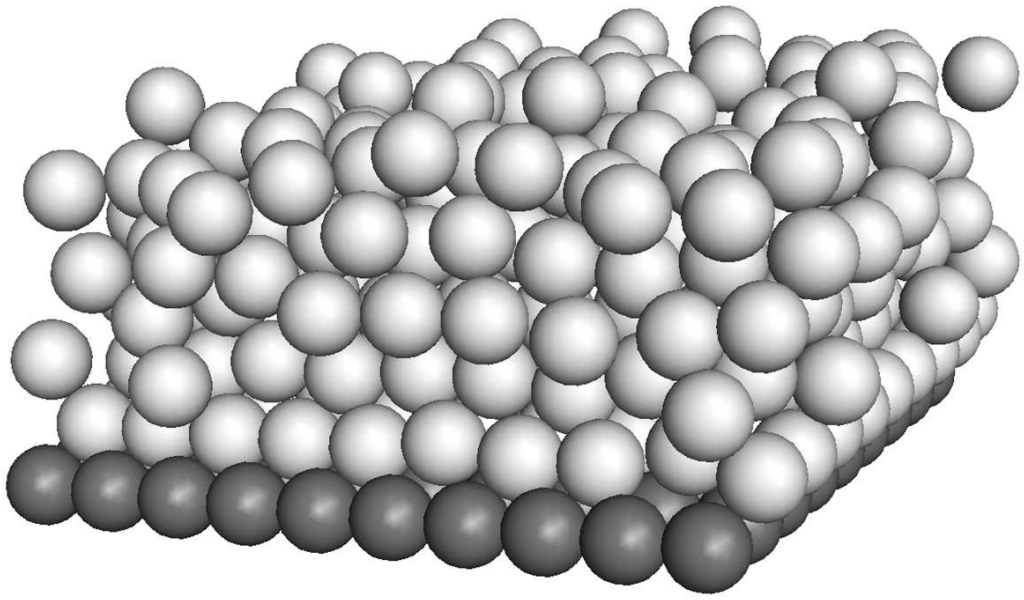

Figure 1 ELJ1064 16JAN2015

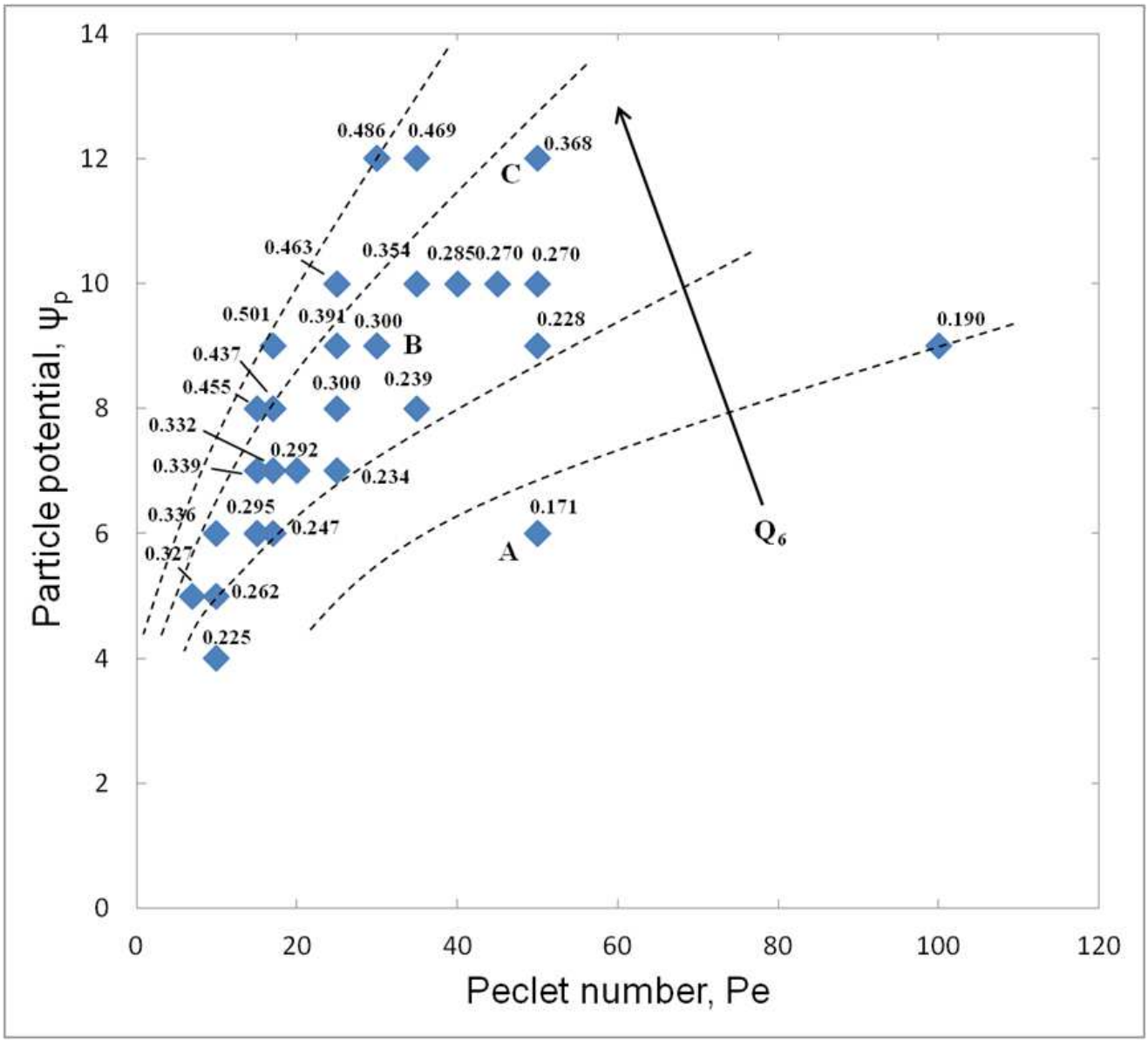

Figure 2a ELJ1064 16JAN2015

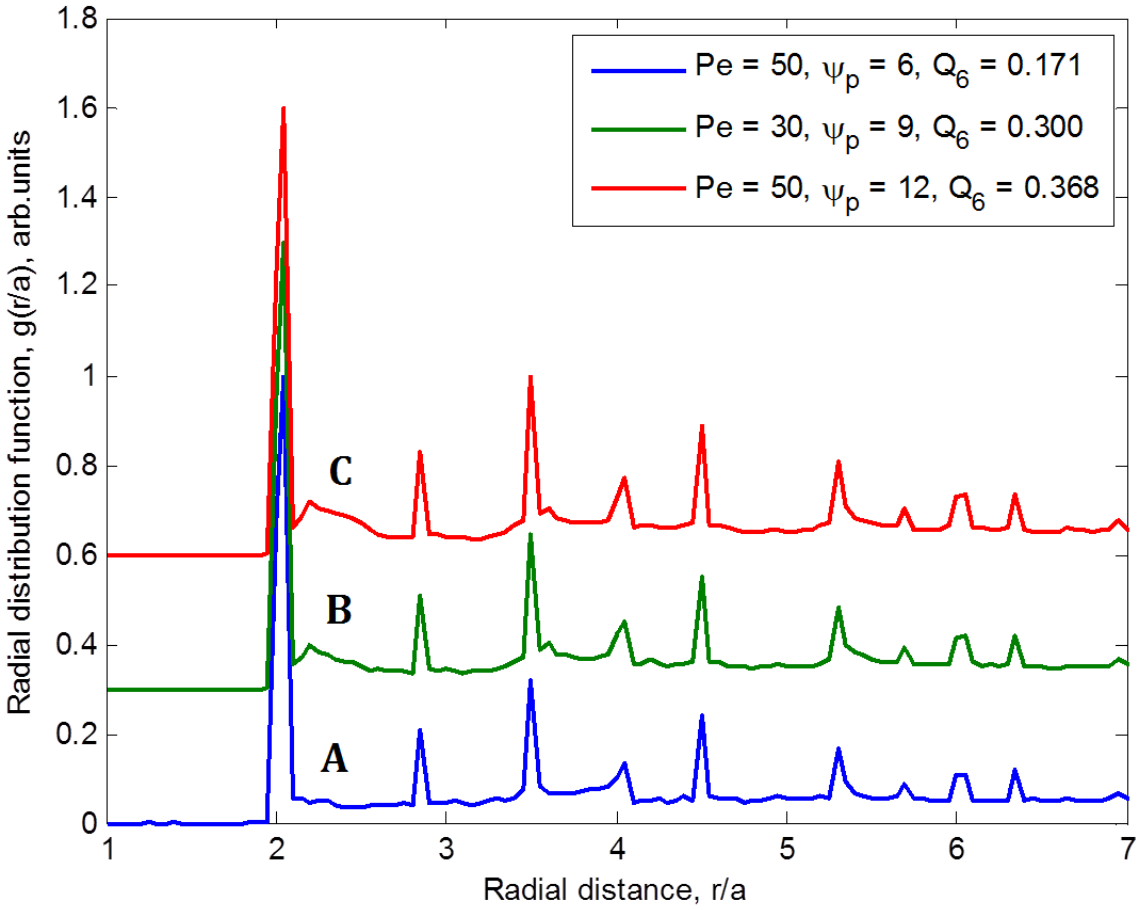

Figure 2b ELJ1064 16JAN2015

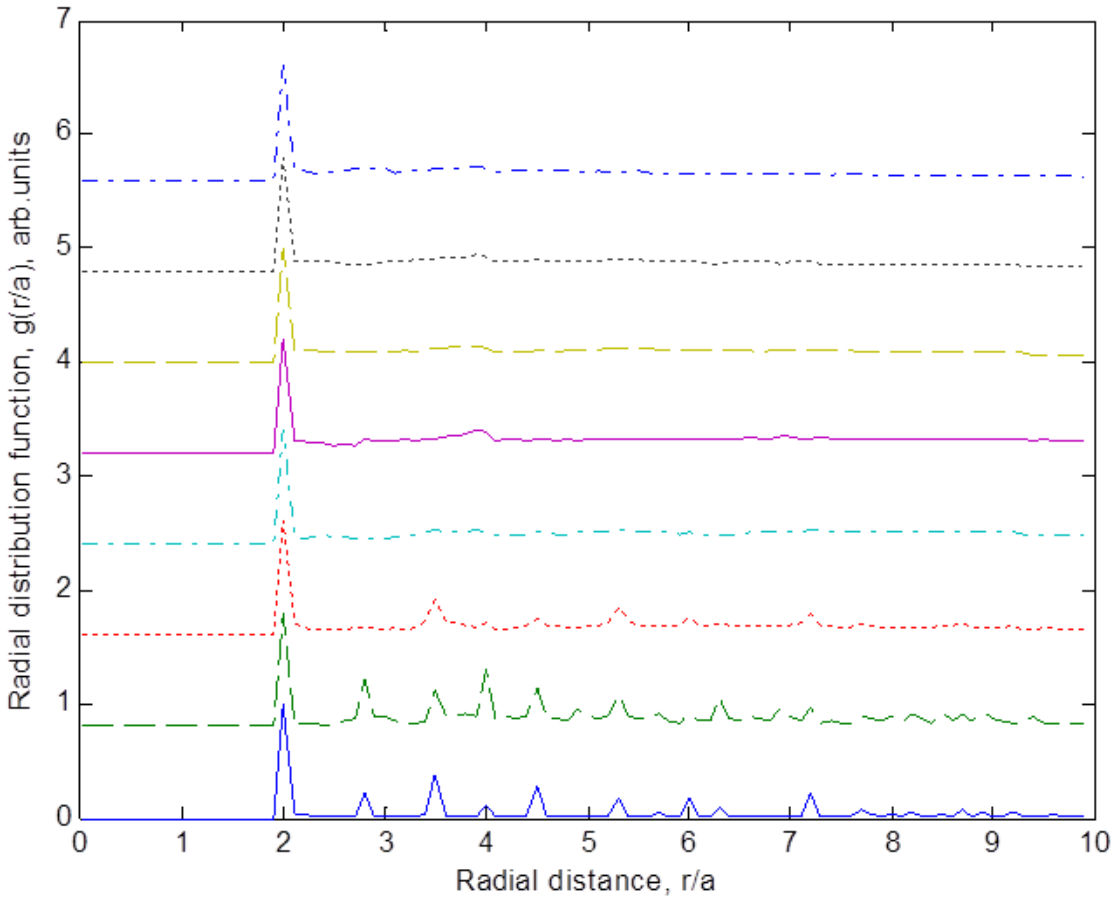

Figure 3a ELJ1064 16JAN2015

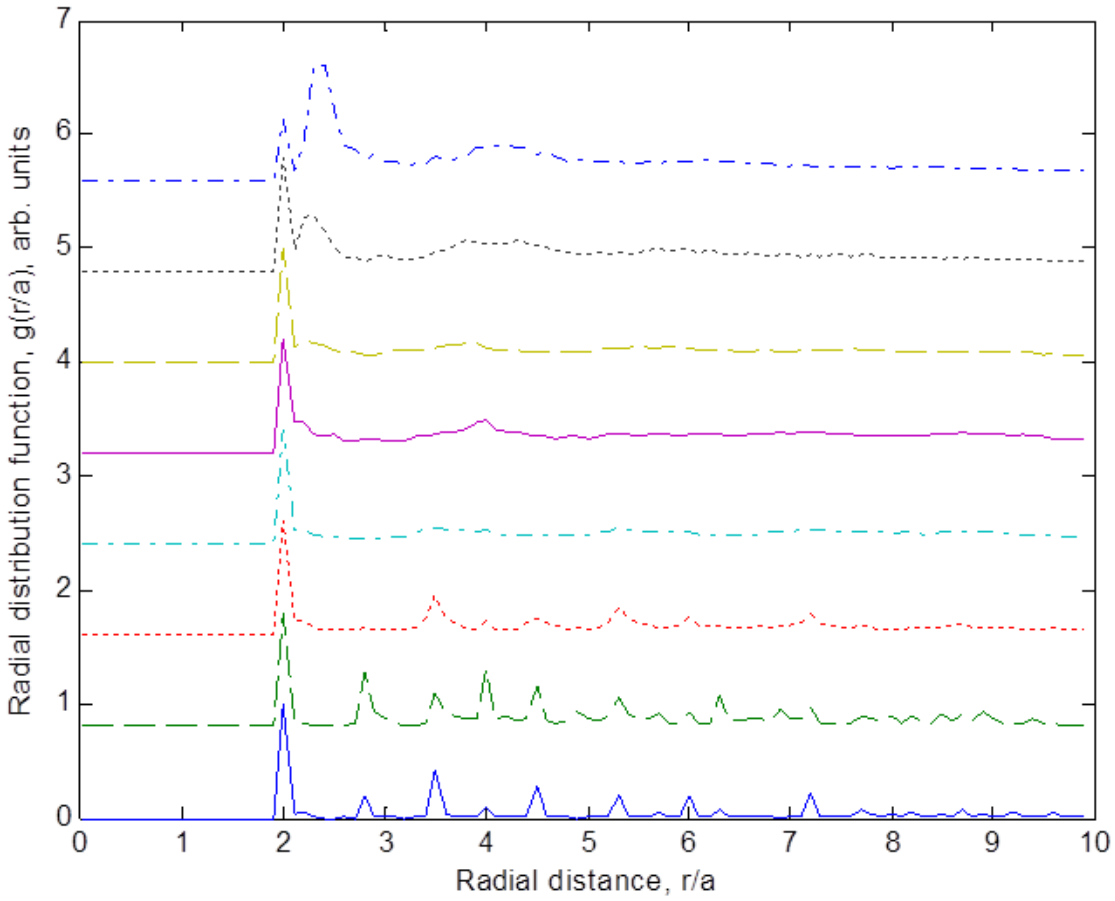

Figure 3b ELJ1064 16JAN2015

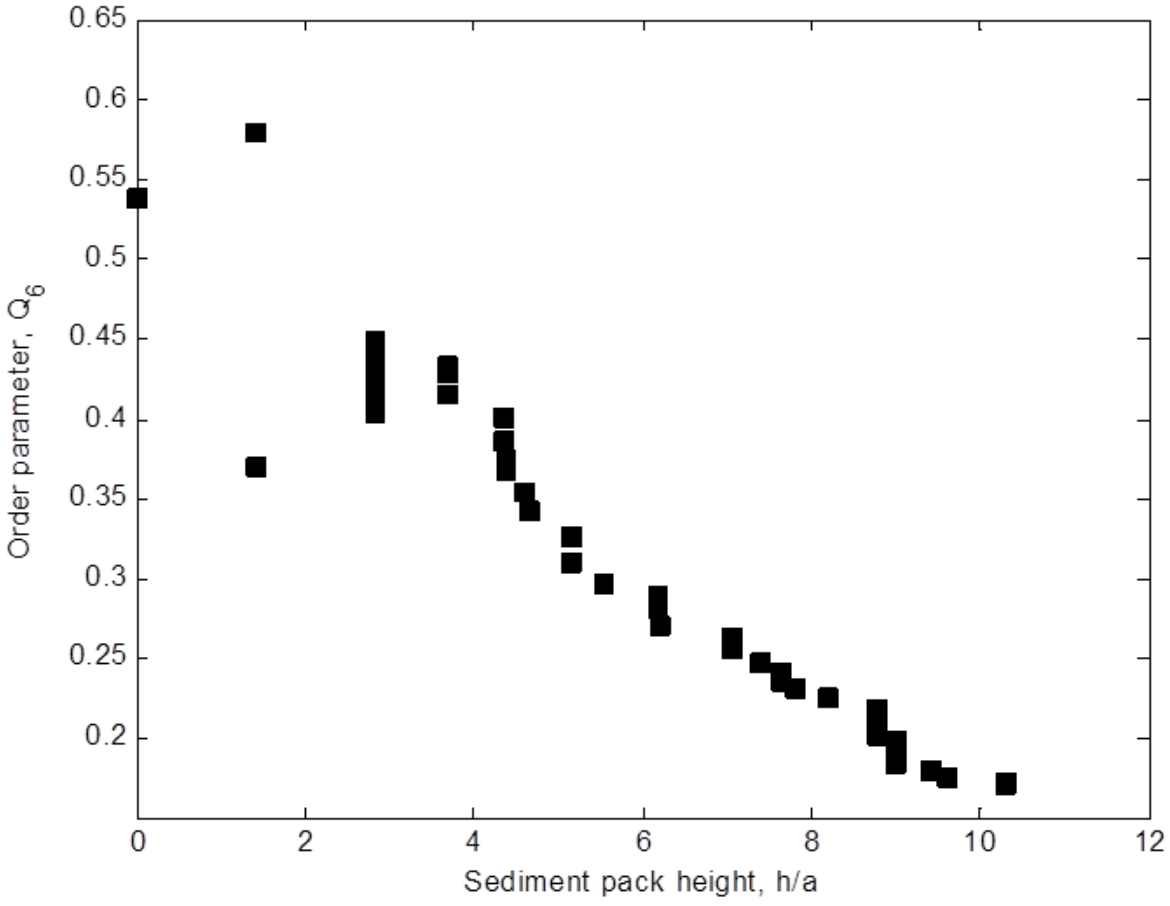

Figure 4a ELJ1064 16JAN2015

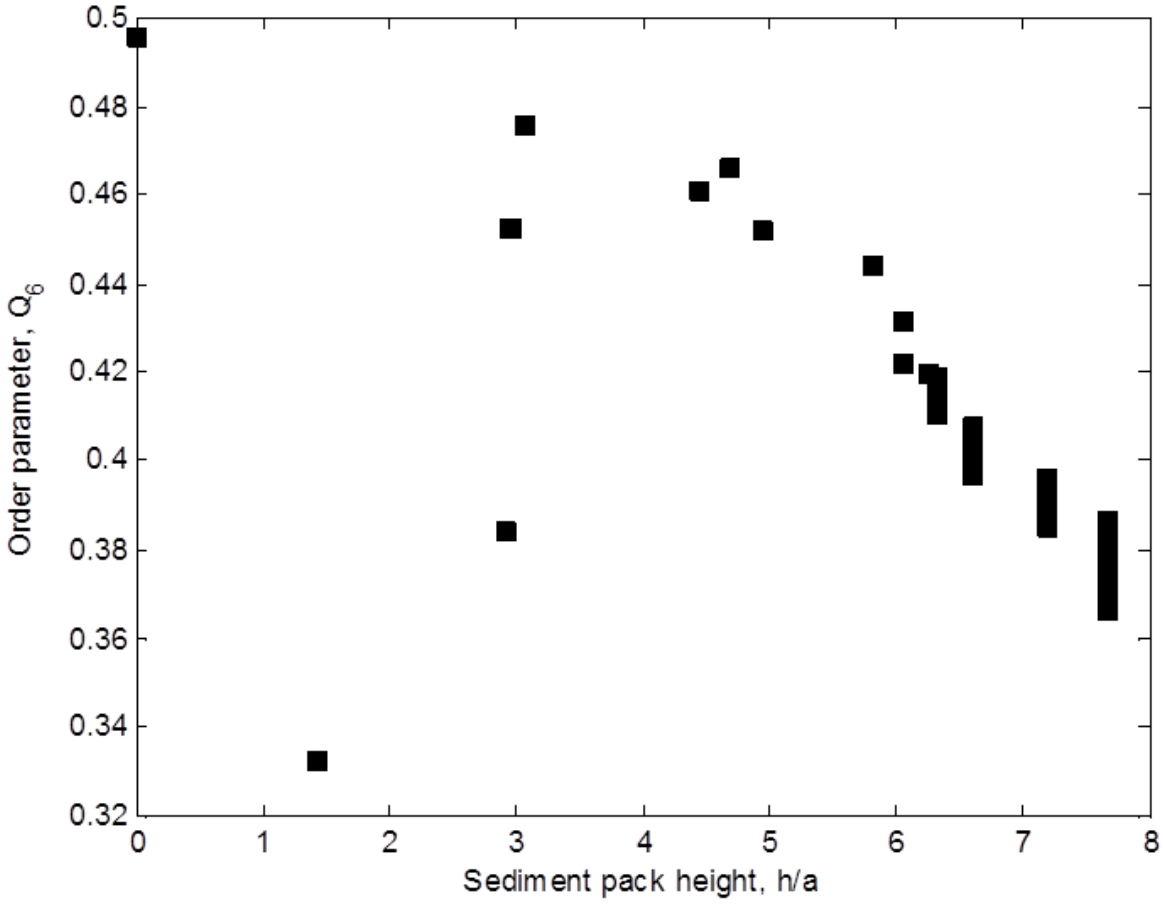

Figure 4b ELJ1064 16JAN2015

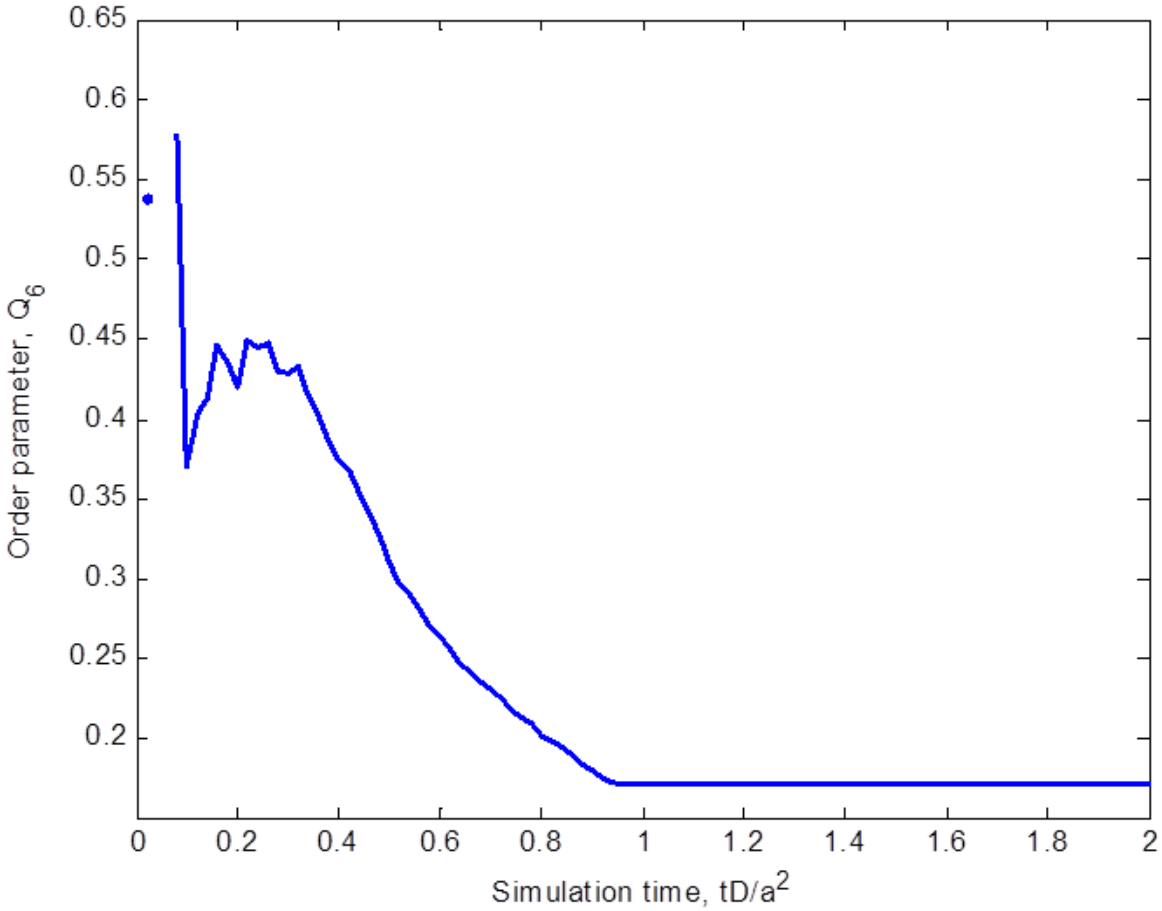

Figure 4c ELJ1064 16JAN2015

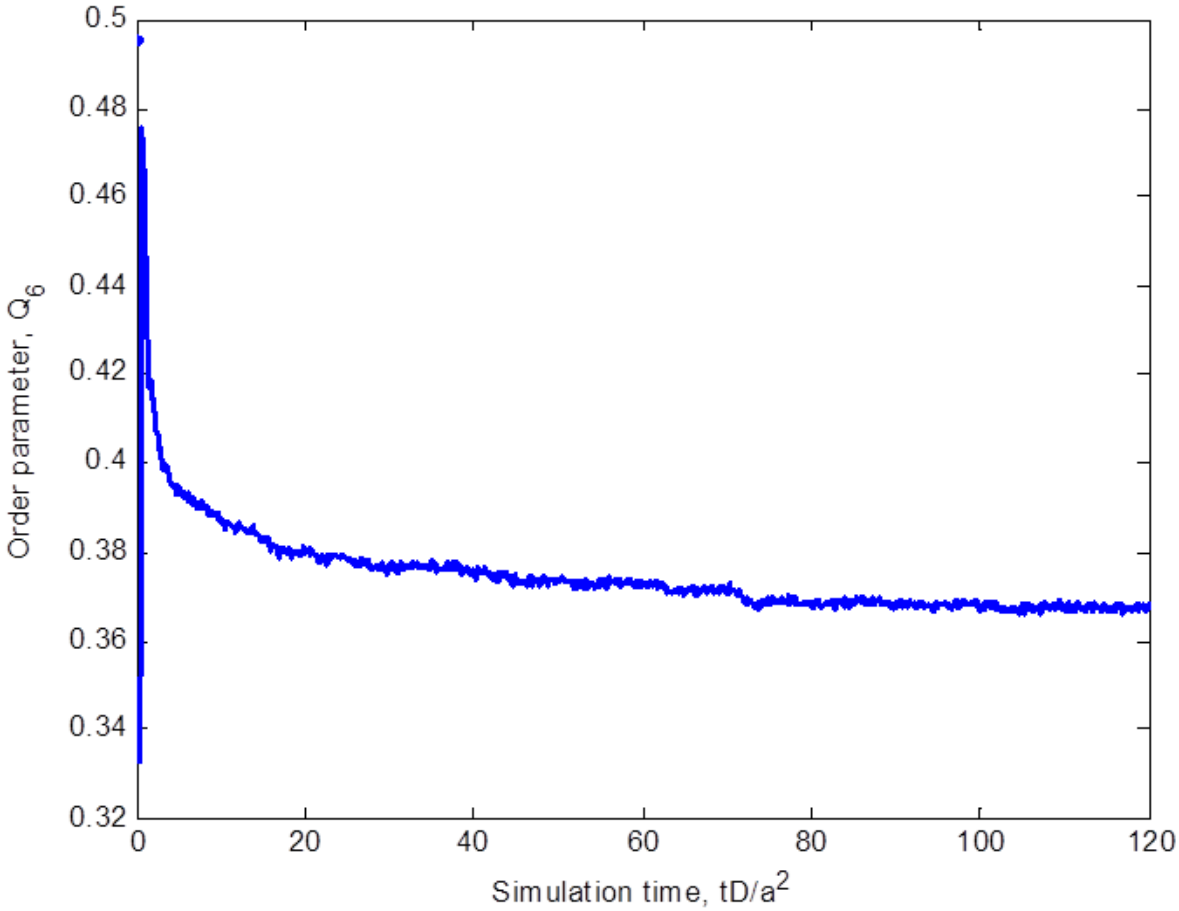

Figure 4d ELJ1064 16JAN2015

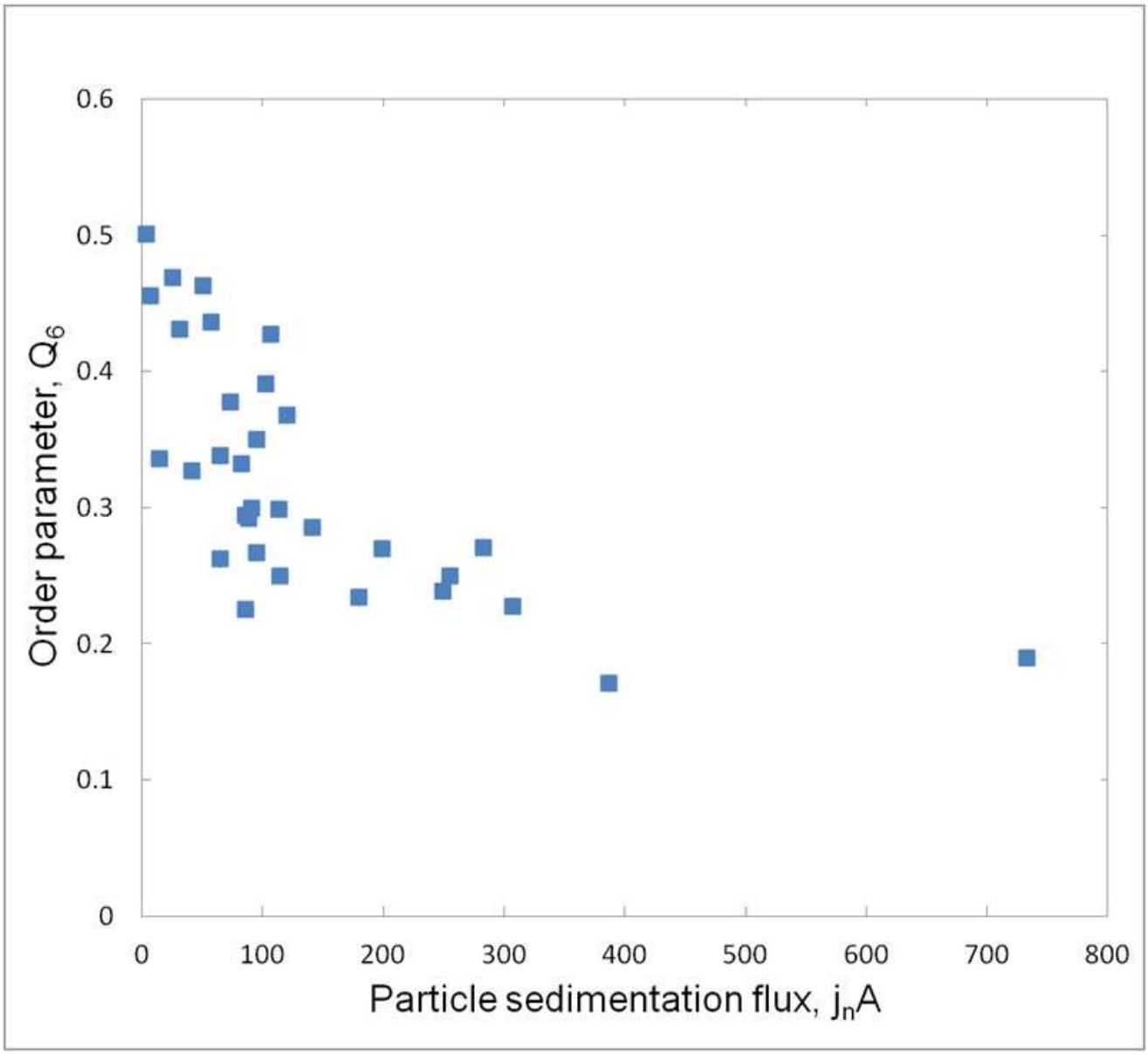

Figure 5 ELJ1064 16JAN2015